

Hybrid Antenna Array for 4G/5G Smartphone Applications

Ming Yang^{1, 2}, Yufa Sun^{2, *}, and Jinzhi Zhou¹

Abstract—In this paper, a hybrid antenna array for 4G/5G smartphone applications is presented. The hybrid antenna system is composed of one array of two antenna elements for 4G application and another array of six antenna elements for 5G application. By loading PIN diodes and changing the on/off state of the PIN switch, then the resonance point will shift. The 2-antenna array broadens the bandwidth of 4G frequency band and is capable of covering GSM850/900/DCS1800/PCS1900/UMTS2100 and LTE2300/2500 operating bands. A U-shape monopole strip and an S-shape slot coupling technologies are also introduced, the 6-antenna array improves the impedance matching for the proposed 5G antenna array and is capable of covering the 5G (3300–3600 MHz and 4800–5000 MHz), which can meet the demand of 5G application. Spatial and polarization diversity techniques are implemented on these antenna elements so that high isolation can be achieved. This hybrid antenna array is fabricated, and typically experimental results such as S_{11} , isolation, radiation pattern efficiency, and channel capacity are presented. The measured results are in good agreement with the simulated ones.

1. INTRODUCTION

In recent years as the 4G communication system becomes mature, many research institutions have shifted their focuses to the next-generation communication (5G) [1–3]. Wireless communication network environment has become a mixture of different kinds of heterogeneous networks. The development of multi-mode mobile terminals has already aroused worldwide attention. In consequence, as a key part for terminal device, multi-mode and multi-band smartphone antenna is becoming increasingly important, especially those with incorporated MIMO system [4–8]. In November 2017, the Ministry of Industry and Information Technology of the People’s Republic of China promulgated the 5G operating license of domestic mobile phones and defined the band division of a new generation of mobile communication. The bands are divided into 3300–3600 MHz and 4800–5000 MHz as future broadband mobile services, which makes the new generation of mobile communication not only feature high frequency and wide band but also be compatible with 2G, 3G, and 4G wireless communication. Therefore, considering the future 5G operation, massive MIMO system based on multi-antennas may be a promising candidate for future terminal devices.

It is well known that most mobile phones with an internal dual-antenna system are designed to cover the LTE/WWAN operation [9–12], which only takes into consideration of 4G frequency bands. In order to satisfy future 5G applications, MIMO antennas for 5G smartphone applications have been discussed in [13–18]. These MIMO antennas could cover the 5G (3300–3600 MHz); however, the bandwidth is too narrow to completely cover the new generation of mobile communication, which is 4800–5000 MHz.

In this paper, a hybrid antenna array is developed to support the GSM850/900, DCS, PCS, UMTS, LTE2300/2500, and 5G (3300–3600 MHz and 4800–5000 MHz) frequencies. The proposed antenna is realized by using a 2-antenna array and a 6-antenna array. All the eight antenna elements are central

Received 12 July 2020, Accepted 4 August 2020, Scheduled 15 September 2020

* Corresponding author: Yufa Sun (yfsun_ahu@sina.com).

¹ Electronics and Information Engineering Department, Bozhou University, Bozhou 236800, China. ² Key Lab of Intelligent Computing & Signal Processing, Ministry of Education, Anhui University, Hefei 230601, China.

symmetrically disposed, which meticulously placed along on the edges of the system ground plane. In Section 2, the configuration of the proposed hybrid antenna array is introduced, and the operating principle is analyzed. In Section 3, the measured S -parameters, gain, efficiency, and radiation patterns of the hybrid antenna are presented and discussed.

2. HYBRID ANTENNA ARRAY STRUCTURE

The geometry of the hybrid antenna array for 4G/5G smartphone application is shown in Fig. 1. The system circuit board is a 0.8 mm thick FR4 substrate with relative permittivity 4.4 and loss tangent 0.02, and the size of the system circuit board is 140 mm \times 65 mm. The system ground plane is printed on the back surface. In order to fit for the demands of smartphone, the total thickness of the antennas is limited to 5 mm. As shown in Fig. 1(a), the two 4G antenna elements are placed along the two short edges of the system ground plane, while the six 5G antenna elements are printed along the two long edges of the system ground plane.

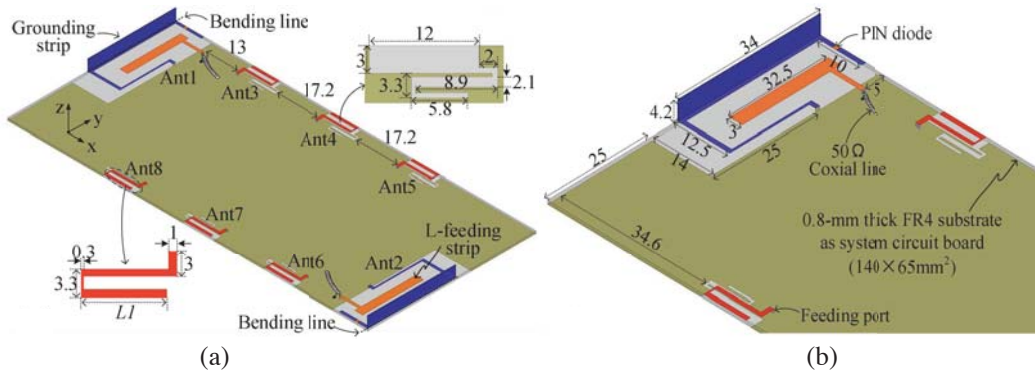


Figure 1. (a) Configuration of proposed antenna. (b) Structure of 4G/5G antenna elements (unit: mm).

2.1. 4G Antenna Array Structure

The 4G antenna structure proposed in this paper is a reconfigurable antenna array that can cover LTE/WWAN operation bands, which is composed of two antenna elements (Ant1 and Ant2), and its detailed structure and optimized dimensions are given in Fig. 1(b). Each antenna element consists of an L-shape feeding strip and a C-shape grounding strip with a PIN diode (BAP64-03), and the positive and negative voltages for PIN diode are supplied through bias lines. Bottom of the C-shaped ground strip is connected to the system ground, while the ground strip is excited by the L-shaped feeding strip. Length of the ground strip is changed by the on/off state of the PIN switch. The length of the ground strip plays an important role in the capacitance of the 4G antenna. The capacitance in the 4G antenna will increase when the ground strip becomes longer. According to [19], the resonant frequency can be simply written as:

$$f_r = \frac{1}{2\pi\sqrt{L_{eff}C_{eff}}} \quad (1)$$

As shown in Equation (1), L_{eff} is the equivalent inductance, and C_{eff} is the equivalent capacitance. The resonant frequency is shifted to lower frequency, due to increased capacitance in the coupled ground strip.

The two antenna elements are far apart from each other which leads to improvement of isolation in the lower bands. The L-shape feeding strip and grounding strip can excite three fundamental resonant modes at 800 MHz, 1700 MHz, and 2400 MHz, respectively, which can cover GSM850/DCS1800/PCS1900/UMTS2100 and LTE2300 frequency bands in the ON state of PIN diode. In addition, when the PIN diode is in the OFF state, the resonant modes at 800 MHz and 2400 MHz

are shifted to 900 MHz and 2550 MHz, respectively, which can cover GSM900 and LTE2500 frequency bands.

To further understand the working mechanism of the 4G antenna, the simulation results of the surface current distributions at the resonant frequencies are illustrated in Fig. 2 and Fig. 3. As shown in Figs. 2 and 3, the surface currents at 850 MHz and 2400 MHz are mainly distributed along the grounding strip. When the PIN diode turns off, the length of the grounding strip becomes shorter. This shifts the two resonances of the lower and higher bands to the right. Since 1700 MHz resonance mode is mainly generated by an L-shape feeding strip, the effect of coupling line loaded with PIN diodes on it is slight and can be negligible, while the resonance of the middle band stays unchanged. In this case, the corresponding bandwidths of these resonances are wide enough to cover the whole frequency bands for LTE/WWAN.

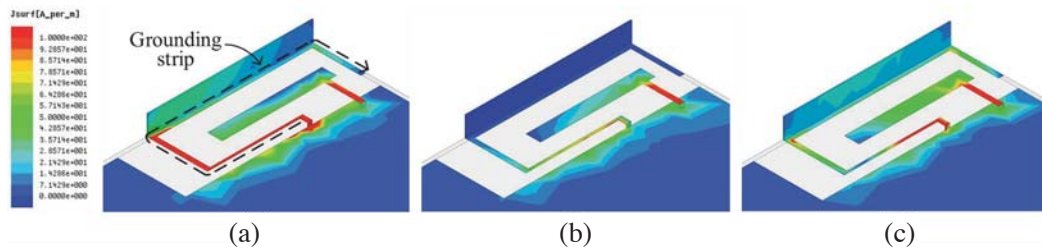


Figure 2. Surface current distribution when the PIN diode is in the ON state: (a) 850 MHz, (b) 1700 MHz and (c) 2400 MHz.

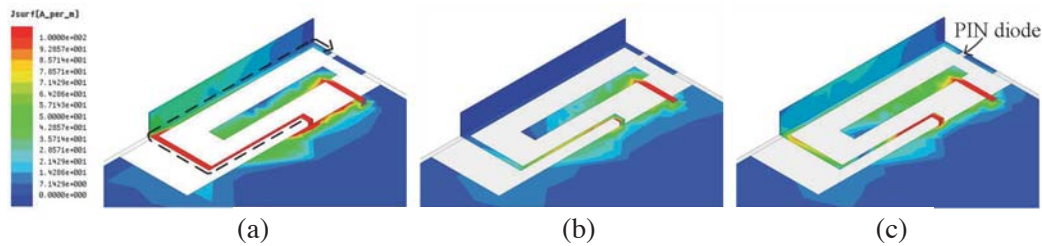


Figure 3. Surface current distribution when the PIN diode is in the OFF state: (a) 900 MHz, (b) 1700 MHz and (c) 2550 MHz.

Figure 4(a) shows the simulated S -parameters of the proposed 4G antenna. As can be seen from Fig. 4(a), a wide bandwidth of 17% (809–962 MHz) for the low band is obtained. Meanwhile, a bandwidth of about 59% (1471–2692 MHz) for the high band is achieved. Therefore, the proposed 4G antenna array can successfully cover the GSM850/900/DCS1800/PCS1900/UMTS2100 and LTE2300/2500 bands with desirable isolation.

2.2. 5G Antenna Structure

Figure 1(a) shows the configuration of the proposed 5G antenna array, and its detail dimensions are also presented. In this figure, the antenna array, namely, antenna elements (Ants) 3 to 8, are printed along the two long side edges of the system circuit board. Six rectangular clearances of 14 mm × 6.3 mm are also reserved for accommodating the proposed 5G antennas. Here, the adjacent two antenna elements located on the same side edge have a spacing of 17.2 mm. Ant3 and Ant6 are 13 mm away from the 4G antenna element, while Ant5 and Ant8 are 34.6 mm away from the top ground edge. Each element of the 5G antenna array is composed of a U-shape monopole strip and an S-shape slot clearance region. All of the 5G antenna elements are excited through 1 mm wide feeding strips which are connected to a 50 Ω SMA connector. In this design, the dimension of the monopole is specifically designed to cover both the 5G bandwidths: 3300–3600 MHz and 4800–5000 MHz.

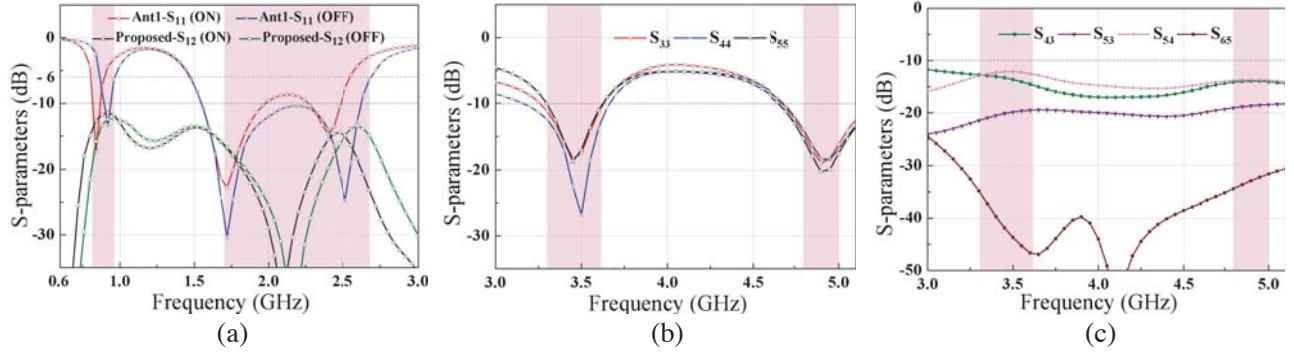


Figure 4. Simulated S -parameters of (a) 4G antenna elements, (b) and (c) 5G antenna elements.

The simulated S -parameters of the proposed 5G antenna elements are shown in Figs. 4(b) and (c). As the left and right side edges of the 5G antenna elements are central symmetrically disposed, only the results of the antenna elements Ant3, Ant4, and Ant5 on the right side edge are presented for brevity. As shown in Fig. 4(b), two resonant modes at approximately 3450 MHz and 4900 MHz are generated, and have good impedance matching of less than -10 dB between 3300–3600 MHz and 4800–5000 MHz. In addition, due to enough distance among elements, good isolation of less than -10 dB is also exhibited between any two antenna elements, as shown in Fig. 4(c).

Figure 5 shows the simulated S_{33} as a function of length $L1$ in the U-shape monopole strip. It is clearly observed that the low- and high-bands are changed as $L1$ varies from 9.1 to 11.1 mm. With the increase of length $L1$, the second resonant mode of high band shifts to lower frequency, and the first resonant mode of low band varies around 3450 MHz. To cover the desired high band, length $L1$ is selected as 10.1 mm. Moreover, the L-shape slot has also improved the impedance matching for the proposed 5G antenna array for lower band. Fig. 6 shows the input impedance in the absence and presence of the L-shape slot. For the lower band, the addition of the L-shape slot decreases the reactance to improve the impedance matching, whose resonant frequency is also excited at about 3400 MHz; therefore, bandwidth of the lower bands is widely enlarged, covering the 3300–3600 MHz band.

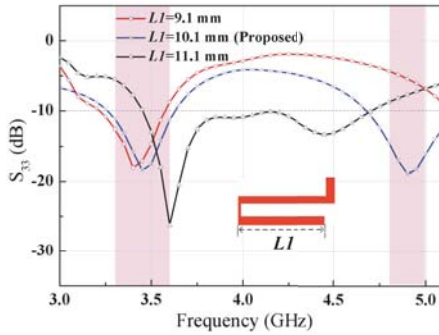


Figure 5. Simulated S_{33} of the Ant3 as a function of $L1$.

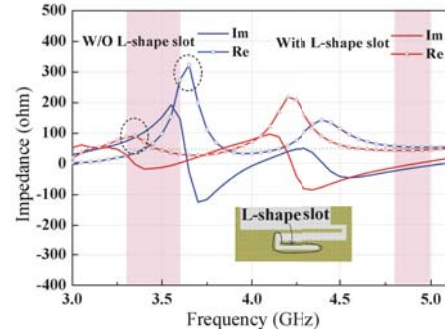


Figure 6. Effects of the L-shape slot on antenna input impedance.

3. MEASURED RESULTS AND DISCUSSION

Based on the hybrid antenna array discussed above, as shown in Fig. 7, a prototype was fabricated and tested. The simulations were performed using the electromagnetic field simulator HFSS version 17, and an Agilent N5247A vector network analyzer was used to measure the S -parameters. Due to identical dimensions and symmetrical placement of the eight array elements, only S -parameters of Ant1, Ant2, Ant3, Ant4, and Ant5 are presented. Finally, the radiating performances such as antenna

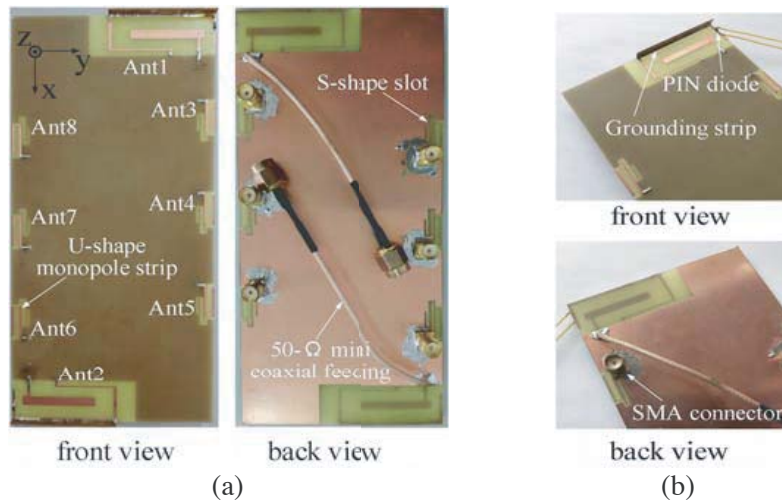


Figure 7. Photographs of the fabricated hybrid antenna array prototype. (a) Overall view. (b) Enlarged view.

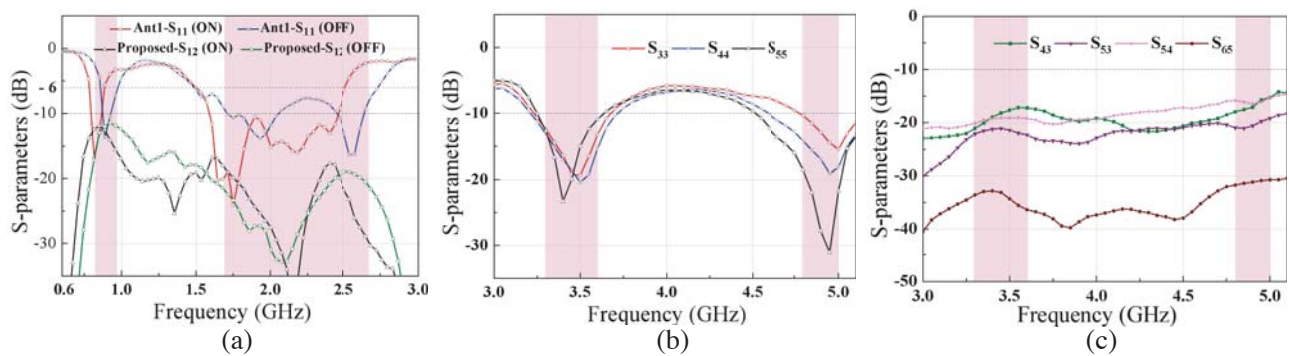


Figure 8. Measured S -parameters of (a) 4G antenna elements, (b) and (c) 5G antenna elements.

gains, radiation efficiencies, and radiation patterns of the proposed hybrid antenna array are given and discussed.

The measured S -parameters of the 4G and 5G antenna elements are presented in Figs. 8(a)–(c), respectively. It is observed that the measured S -parameters are well validated with the simulated ones shown in Fig. 4. The slight differences are possibly due to connector effects, fabrication tolerances, and other uncertain losses. As shown in Fig. 8(a), the 4G antenna elements exhibit desirable measured -6 dB impedance bandwidths of 21% (779–971 MHz) and 57% (1496–2755 MHz), and measured isolation better than -10 dB in both desired frequency bands. As for the measured S -parameters of 5G antenna elements shown in Fig. 8(b), Ant5 shows a minimum measured -10 dB impedance bandwidth of approximately 11% (3246–3640 MHz) and 14% (4516–5183 MHz), while Ant3 and Ant4 show impedance bandwidths which can also cover the 5G operating band. Fig. 8(b) only shows the isolation between major antenna elements, and the measured results of S_{43} , S_{54} , S_{53} , and S_{65} across the 5G are better than -15 dB.

The radiation efficiencies and gains of Ant1, Ant3, Ant4, and Ant5 are shown in Fig. 9. The measured 4G antenna (Ant1) efficiencies over the lower and upper bands are more than 42% and 50%, respectively, while their corresponding antenna gains vary from about 1.1 to 1.76 dBi and 2.7 to 3.9 dBi, respectively. Within the desired 5G frequency band (3300–3600 MHz and 4800–5000 MHz), the measured antenna efficiencies are about 52%–65%, while their corresponding antenna gains are approximately 1.6–2.8 dBi. The proposed hybrid antenna array could meet the general requirement for smartphone antennas.

Figure 10 shows the measured two-dimensional radiation patterns of 4G antenna element Ant1 at

850 and 2400 MHz. Based on the direction of the antenna placement in Fig. 7, the co-pol (E_θ) and cross-pol (E_ϕ) in the xoy -, yoz -, and xoz -planes are measured. According to Fig. 10, E_θ varies smoothly, and it presents omnidirectional radiation, which is advantageous for practical smartphone applications. Fig. 11 shows the measured two-dimensional radiation patterns of Ant3, Ant4, and Ant5 at 3450 MHz

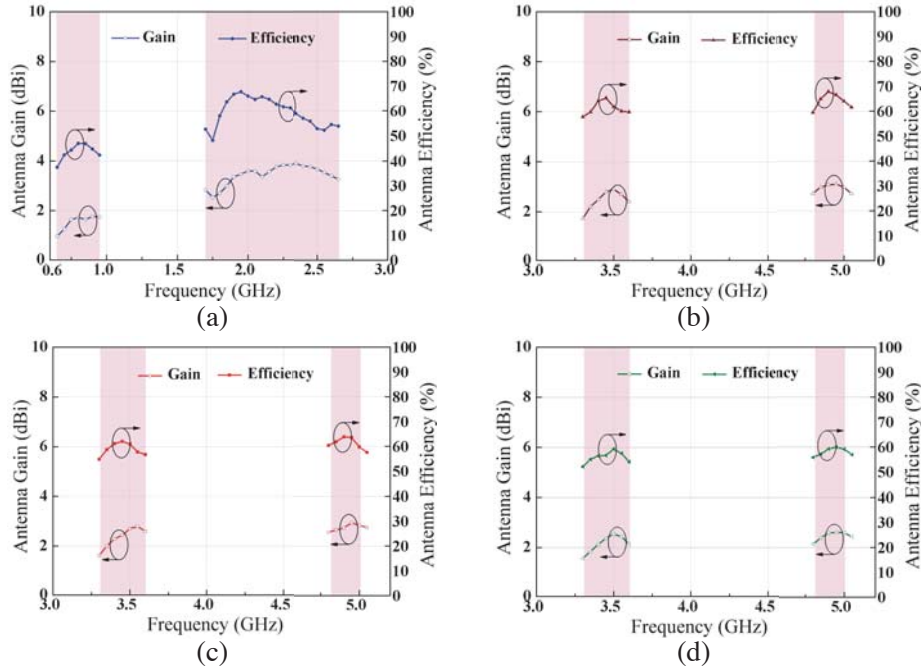


Figure 9. Measured gains and radiation efficiencies of proposed hybrid antenna elements. (a) Ant1. (b) Ant3. (c) Ant4. (d) Ant5.

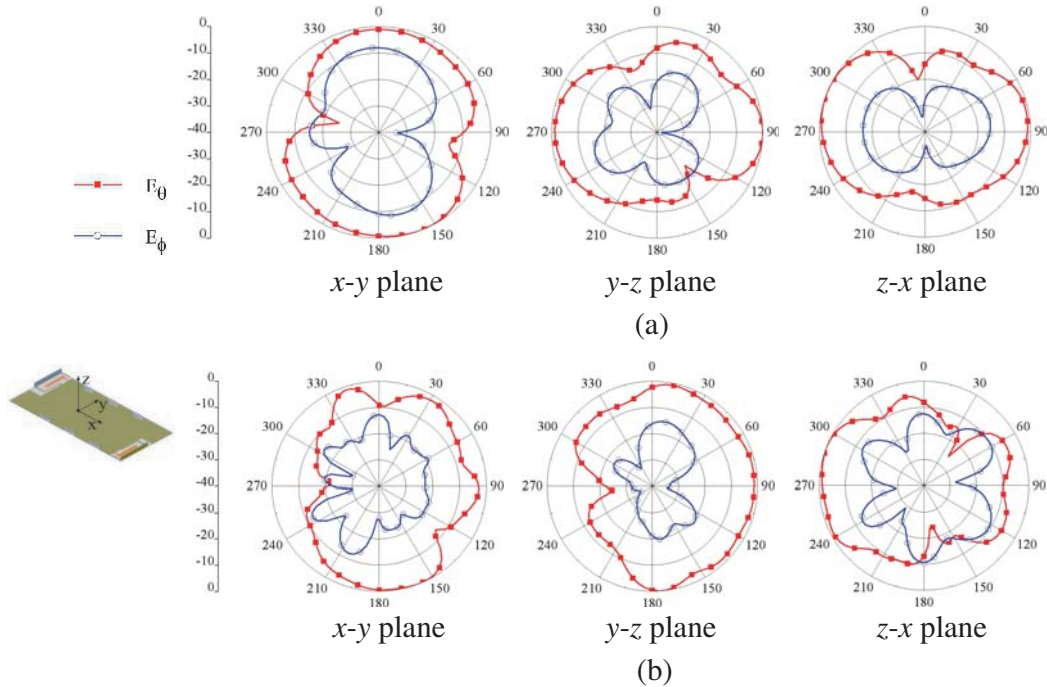


Figure 10. Measured radiation patterns of 4G antennas at (a) 850 MHz, (b) 2400 MHz.

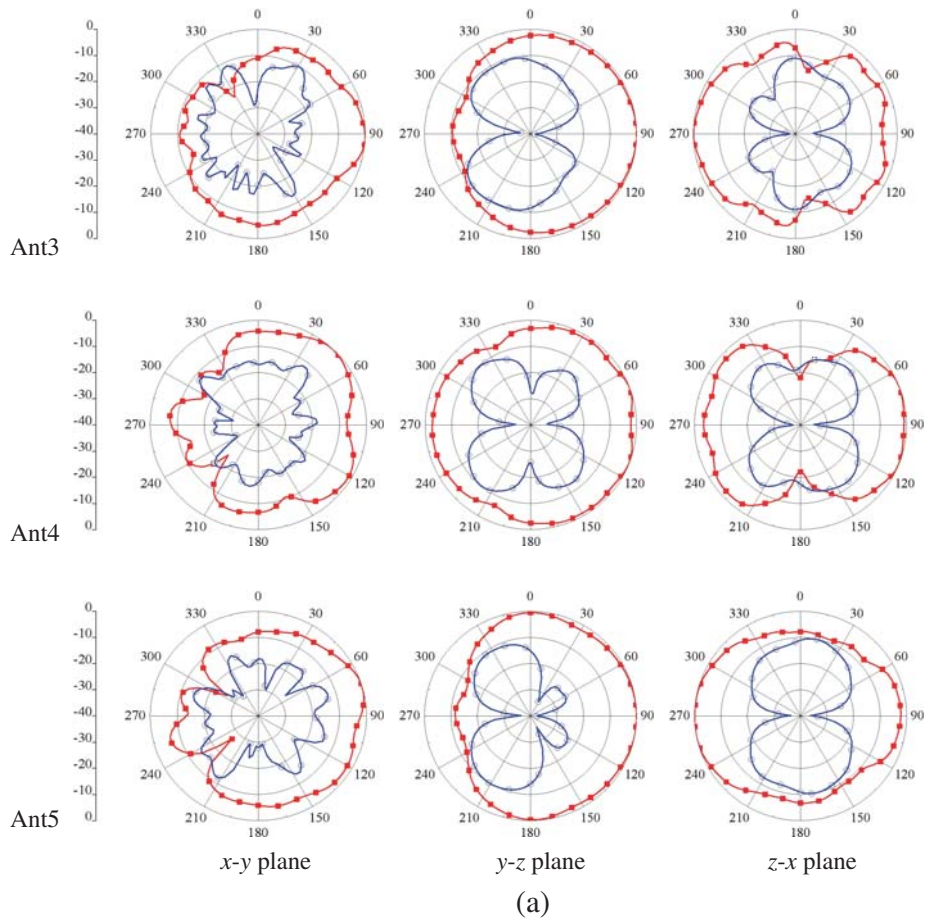
and 4900 MHz. As expected, each 5G antenna element exhibits similar radiation patterns in the three principal planes, in which near bi-directional patterns are observed in the xoz -plane, while both xoy - and yoz -planes demonstrate broadside patterns in the $+Y$ (90°) direction. By comparing E_θ and E_ϕ , it is indicated that a full coverage area in free space can be guaranteed for practical mobile communication applications.

The ergodic channel capacity of the hybrid antenna array is also studied, which can be defined as follows:

$$C = E \left\{ \log_2 \left[\det \left(\mathbf{I}_M + \frac{\text{SNR}}{M} \mathbf{H}\mathbf{H}^H \right) \right] \right\} \quad (2)$$

The E in Eq. (2) denotes the expectation with respect to different channel realisations; \mathbf{I}_M is an identity matrix; SNR is the signal-to-noise ratio at the receiving side; M is the number of transmitting antennas; \mathbf{H} is the channel matrix; and $(\cdot)^H$ denotes the Hermitian transpose. It is assumed that the transmitting antennas are uncorrelated (ECC = 0 at transmitting side) and lossless (total efficiency = 100%), in which the entries are independent identically distributed complex Gaussian variables. The calculated ergodic channel capacities are averaged over 10,000 Rayleigh fading realisations with the SNR of 20 dB. As shown in Figs. 12(a) and (b), the channel capacities of the 2-antenna array and 6-antenna array are 8.8–10.1 bps/Hz and 30.1–30.6 bps/Hz, respectively. Therefore, based on the calculated channel capacity presented above, the proposed hybrid antenna array with excellent performances can be applied in MIMO system.

In addition, a comparison between the proposed antenna and the typical reported smartphone applications according to the antenna number, frequency band, bandwidth, isolation, gain, and efficiency is shown in Table 1. The proposed antenna not only covers the 4G frequency band, but also completely covers all the 5G frequency bands, which is rare in the existing literature. Thus, it can be concluded that the proposed hybrid antenna array with four frequency bands and high isolation up to 10 dB is more suited for 4G/5G smartphone applications.



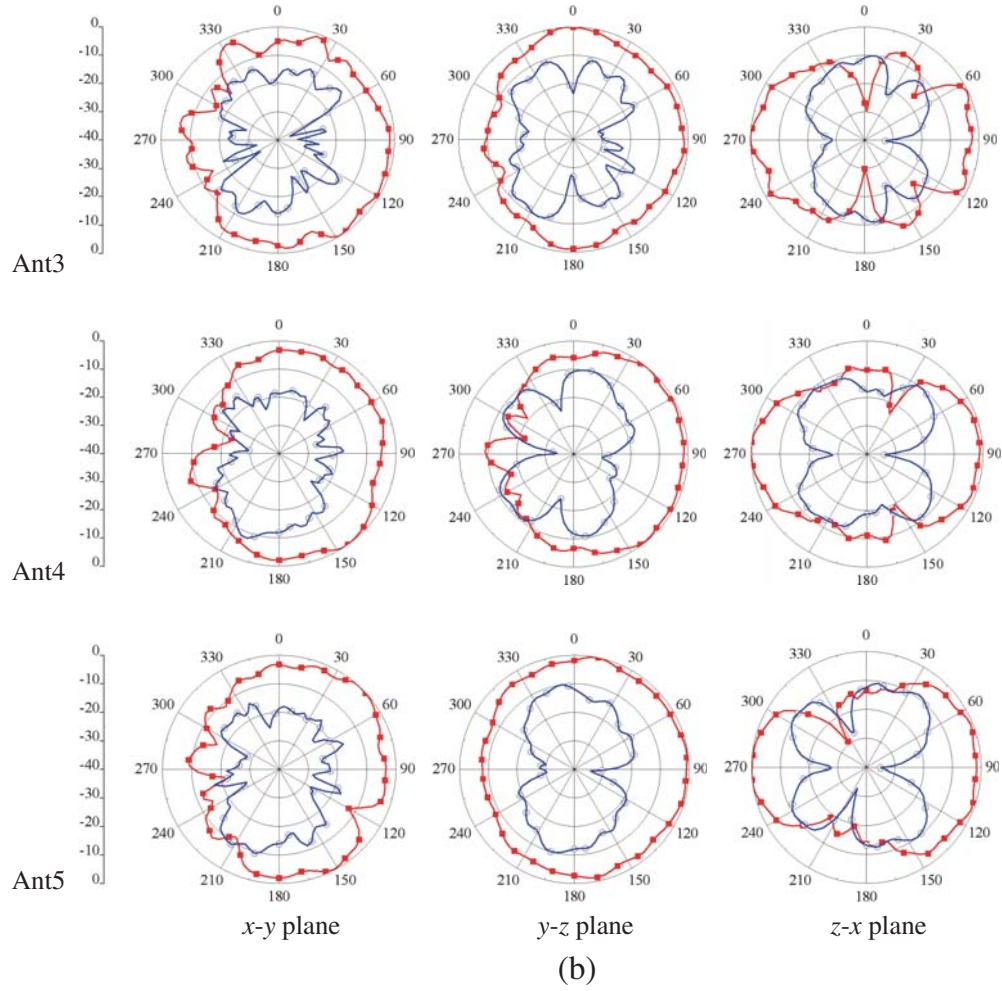


Figure 11. Measured radiation patterns of 5G antennas at (a) 3450 MHz, (b) 4900 MHz.

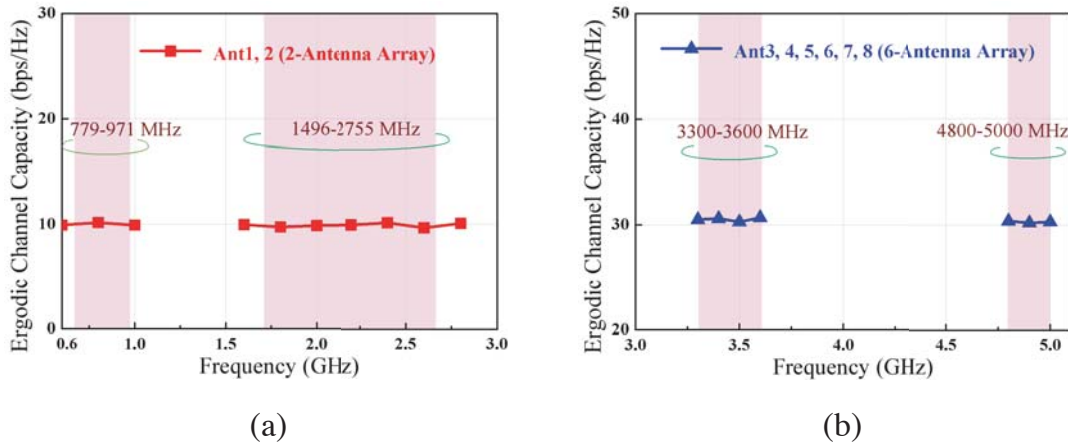


Figure 12. Calculated ergodic channel capacity of hybrid proposed antenna array. (a) 2-antenna array. (b) 6-antenna array.

Table 1. Comparison of proposed antenna and reference antennas.

Reference	Antenna number	Frequency band	Bandwidth (MHz)	Isolation (dB)	Gain (dBi)	Efficiency (%)
[5]	12	mono-band	3400–3600	> 12.5	–	> 50
[6]	10	di-band	3400–3800/ 5150–5925	> 11	–/–	42–65/ > 62–82
[7]	8	di-band	3000–5000	> 21/> 12	–	58.9–88.6/ 31.6–76.7
[10]	2	Octa-band	740–965/ 1380–2703	> 10	0.764–4.505	40–67.2
[13]	8	mono-band	3400–3600	> 10	–	50–60
[14]	8	mono-band	2550–2650	> 12.5	4.79–5.9	53–63
[17]	8	mono-band	3300–3600	> 15	< 4.3	> 40
[18]	8	di-band	3300–6000	> 18	–/–	40–90
Proposed	8	Nona-band	779–971/ 1496–2755/ 3300–3600/ 4800–5000	>10/>15	1.1–3.9/1.6–2.8	42–50 /52–65

4. CONCLUSION

This work has successfully reported a hybrid antenna array composed of 4G and 5G antenna modules, which can be applied to 4G/5G applications. The 4G antenna array with two antenna elements can cover two wide operating bands of 779–971 MHz and 1496–2755 MHz with S_{11} less than -6 dB. The 5G antenna array with six antenna elements can cover the bands of 3300–3600 MHz and 4800–5000 MHz with S_{11} less than -10 dB for communication. Typical results such as S -parameters, radiation efficiency, gain, and radiation pattern are measured, and they can meet the requirements of MIMO systems. In conclusion, the proposed hybrid antenna array can be a suitable candidate for 4G/5G smartphone applications.

ACKNOWLEDGMENT

This work was supported by the National Natural Science Foundation of China under Grant No. 61172020 and the Key Project of Natural Science Research of Colleges and Universities in Anhui Province under Grant No. KJ2018A0818.

REFERENCES

1. Bang, J. and J. Choi, “A SAR reduced mm-wave beam-steerable array antenna with dual-mode operation for fully metal-covered 5G cellular handsets,” *IEEE Antennas and Wireless Propagation Letters*, Vol. 17, No. 6, 1118–1122, Jun. 2018.
2. Sharawi, M. S., M. Ikram, and A. Shamim, “A two concentric slot loop based connected array MIMO antenna system for 4G/5G terminals,” *IEEE Transactions on Antennas and Propagation*, Vol. 65, No. 12, 6679–6686, Dec. 2017.
3. Guo, J. L., L. Cui, C. Li, et al., “Side-edge frame printed eight-port dual-band antenna array for 5G smartphone applications,” *IEEE Transactions on Antennas and Propagation*, Vol. 66, No. 12, 7412–7417, Dec. 2018.

4. Choi, J., W. Hwang, C. You, et al., "Four-element reconfigurable coupled loop MIMO antenna featuring LTE full-band operation for metallic-rimmed smartphone," *IEEE Transactions on Antennas and Propagation*, Vol. 67, No. 1, 99–107, Jan. 2019
5. Li, M. Y., Y. L. Ban, Z. Q. Xu, et al., "Tri-polarized 12-antenna MIMO array for future 5G smartphone applications," *IEEE Access*, Vol. 5, 6160–6170, 2017.
6. Li, Y. X., C. Y. D. Sim, Y. Luo, et al., "Multi-band 10-antenna array for sub-6 GHz MIMO applications in 5G smartphones," *IEEE Access*, Vol. 6, 28014–28053, 2018.
7. Sun, L. B., Y. Li, Z. J. Zhang, and Z. H. Feng, "Wideband 5G MIMO antenna with integrated orthogonal-mode dual-antenna pairs for metal-rimmed smartphones," *IEEE Transactions on Antennas and Propagation*, Vol. 68, No. 4, 2494–2503, Apr. 2020.
8. Rahmi, B. I. R. and K. L. Wong, "Integrated inverted-F and open-slot antennas in the metal-framed smartphone for 2×2 LTE LB and 4×4 LTE M/MB MIMO operations," *IEEE Transactions on Antennas and Propagation*, Vol. 66, No. 10, 5004–5012, Oct. 2018.
9. Wang, S. and Z. W. Du, "Decoupled dual-antenna system using crossed neutralization lines for LTE/WWAN smartphone applications," *IEEE Antennas and Wireless Propagation Letters*, Vol. 14, 523–526, 2015.
10. Dong, J., X. Yu, and L. Deng, "A decoupled multiband dual-antenna system for WWAN/LTE smartphone applications," *IEEE Antennas and Wireless Propagation Letters*, Vol. 16, 1528–1532, 2017.
11. Wang, S. and Z. W. Du, "A dual-antenna system for LTE/WWAN/WLAN/WiMAX smartphone applications," *IEEE Antennas and Wireless Propagation Letters*, Vol. 14, 1443–1446, 2015.
12. Ban, Y. L., Z. X. Chen, Z. Chen, et al., "Decoupled closely spaced heptaband antenna array for WWAN/LTE smartphone applications," *IEEE Antennas and Wireless Propagation Letters*, Vol. 13, 31–34, 2014.
13. Wong, K. L., C. Y. Tsai, and J. Y. Lu, "Two asymmetrically mirrored gap-coupled loop antennas as a compact building block for eight-antenna MIMO array in the future smartphone," *IEEE Transactions on Antennas and Propagation*, Vol. 65, No. 4, 1765–1778, 2017.
14. Li, M. Y., Y. L. Ban, Z. Q. Xu, et al., "Eight-port orthogonally dual-polarized antenna array for 5G smartphone applications," *IEEE Transactions on Antennas and Propagation*, Vol. 64, No. 9, 3820–3830, Sep. 2016.
15. Li, M. Y., Z. Q. Xu, Y. L. Ban, et al., "Eight-port orthogonally dual-polarised MIMO antennas using loop structures for 5G smartphone," *IET Microwaves Antennas and Propagation*, Vol. 11, No. 12, 1810–1816, 2017.
16. Wong, K. L. and J. Y. Lu, "3.6-GHz 10-antenna array for MIMO operation in the smartphone," *Microwave and Optical Technology Letters*, Vol. 57, No. 7, 1699–1704, 2015.
17. Jiang, W., B. Liu, Y. Q. Cui, and W. Hu, "High-isolation eight-element MIMO array for 5G smartphone applications," *IEEE Access*, Vol. 7, 34104–34112, 2019.
18. Yuan, X. T., W. He, K. D. Hong, et al., "Ultra-wideband MIMO antenna system with high element-isolation for 5G smartphone application," *IEEE Access*, Vol. 8, 56281–56289, 2020.
19. Ban, Y. L., Y. F. Qiang, G. Wu, et al., "Reconfigurable narrow-frame antenna for LTE/WWAN metal-rimmed smartphone applications," *IET Microwaves Antennas and Propagation*, Vol. 10, No. 10, 1092–1100, 2016.